Non-spherical particle stabilised emulsions formed through emulsion destabilisation and arrested coalescence

Benjamin T. Lobel[1*], Daniele Baiocco[2], Mohammed Al-Sharabi[3], Alexander F. Routh[3], Zhibing Zhang[2], Olivier J. Cayre[1*]

[1]School of Chemical and Process Engineering, University of Leeds, Leeds, LS2 9JT, United Kingdom

[2]School of Chemical Engineering, University of Birmingham, Birmingham, B15 2TT, United Kingdom

[3]Department of Chemical Engineering and Biotechnology, University of Cambridge, Cambridge, CB2 3RA, Cambridge, United Kingdom

*Corresponding Author: b.t.lobel@leeds.ac.uk

*Corresponding Author: o.j.cayre@ leeds.ac.uk

Abstract

Hypothesis

To form non-spherical emulsion droplets the interfacial tension driving sphericity must be overcome. This can be achieved through particle jamming at the interface, however careful particle coverage is required. By forming interfacially active particles during emulsion destabilisation, it is expected that non-spherical droplets may be formed via a simple batch process. Furthermore, by increasing the electrolyte concentration the degree of anisotropy should increase.

Experiments

Oil-in-water emulsions stabilised by surfactant in the presence of dopamine were produced. These emulsions were treated with tris(hydroxymethyl)aminomethane hydrochloride buffer to simultaneously initiate polymerisation of dopamine and reduce the Debye length of the system, accelerating droplet coalescence. The concentration of the buffer and the shear were then systematically varied and the behaviour at the interface studied using pendent drop tensiometry and interfacial shear rheology.

Findings

Polydopamine nanoparticles adsorbed to the reducing interface resulting in anisotropic droplets formed via arrested coalescence. The incidence of droplet non-sphericity increased as a function of the electrolyte concentration. Greater shear rates resulted in accelerated coalescence, and formation of secondary droplets, lower shear rates resulted in thicker interfacial films. Stability of these emulsions was due to the formation of an interfacial film resulting from a combination of particle and oligomer interactions at the interface.

Keywords: Emulsions, Anisotropy, Non-spherical, Interfacial, Adsorption, Pickering Emulsion, Coalescence, Polydopamine, Polypyrrole.

1. Introduction

Non-spherical or anisotropic emulsions may be beneficial in a number of applications owing to their increased surface area to volume ratio, including in catalysis, pharmaceuticals, nutrition and as templates for microencapsulation [1-6]. This increase in surface area may result in increased target-adsorption efficiency and a reduction in material requirements to achieve desired effects [7-10]. In

order to achieve non-spherical emulsions, the surface tension, driving both the reduction in interfacial area and consequently the droplet sphericity, must be overcome. This has previously been achieved in the contemporary literature for emulsion droplets but also for particles. For example, Roh et al produced soft dendritic particles that demonstrated high substrate adhesion [11]. However, this method required careful tuning of solvent-polymer interactions and shear flow conditions. Likewise, Procter and Gamble have patented technology utilising the internal freezing of an oil structure via in-situ crystallisation under shear, resulting in anisotropic surfactant-stabilised emulsions developed for enhanced substrate adhesion and active delivery [12]. In this case, the mechanical attributes imparted by the crystallised wax resist the restoring force of surface tension. Recently, Lian et al have produced non-spherical emulsions via coaxial flow and fast interfacial polymerisation of butylcyanoacrylate resulting in ellipsoidal droplets [13]. Non-spherical emulsion droplets have also been formed using particle stabilised emulsions. Particle stabilised emulsions differ from traditional surfactant emulsions as their primary stabilization is typically driven by steric interactions, resulting from irreversible particle adsorption on the droplet surface. The energy required to desorb a particle from the interface (ΔE) is a function of the particle radius (R), the contact angle (θ), and the bare aqueous/oil interfacial tension (γ_{ow})[14, 15] and may be calculated using:

$$\Delta E = \pi R^2 \gamma_{ow} (1 \pm \cos\theta)^2 \qquad (1)$$

where desorption energy is minimised at very low or high values of θ, ie, where the particle is easily desorbed from the interface into the water phase or oil phase, respectively. When the energy of desorption is high and, as a result, the particles can be considered as irreversibly adsorbed, if particle stabilised emulsions are partially covered and begin to coalesce, they may undergo arrested coalescence, a process by which there is insufficient surface area on the newly formed (larger) droplet to accommodate all of the adsorbed particles, thus causing interfacial jamming. This jamming results in a mechanical resistance to complete the coalescence process, driving non-spherical droplet shapes [16-20].

A benefit of producing anisotropic particle-stabilised emulsions is the relative ease with which they may be further developed into microcapsules, providing protection of active ingredients not available to a simple emulsion system [6]. Bon and coworkers were able to produce non-spherical droplets by forcing laponite-stabilised droplet coalescence through a narrow capillary, while Subramaniam et al reported the formation of anisotropic particle-stabilised bubbles by pressing partially coated bubbles together between two glass slides [19, 20]. Another reported method for forming non-equilibrium shapes in particle stabilised emulsions is via nanoparticle surfactants. These systems are comprised of particles made surface active via electrostatic interfacial interactions with an oppositely-charged species in the opposite phase. Such systems have been shown to form non-spherical emulsions and simple bijels, but typically require carefully chosen polymer, particle and solvent combinations [21, 22]. These aforementioned methods, while effective, require the use of specialist equipment, specific material interactions or are only capable of producing droplets sequentially, which may result in challenging scale-up.

Herein we report the formation of non-spherical emulsions stabilised by a combination of surfactants and polymer nanoparticles via a simple and scalable process with no requirement for bespoke or specialist equipment or techniques. These emulsions are formed via in-situ polymerisation during electrolyte induced emulsion destabilisation/coalescence. By exploiting the coalescence of a destabilising emulsion and the kinetics of a chemical oxidative polymerisation process, the interface of coalescing droplets can be intentionally jammed resulting in anisotropic particle-stabilised emulsions. In developing these systems, we investigate the impact of the destabilising electrolyte concentration and the shear rate during the coalescence/polymerisation processes. Furthermore, we show that anisotropic emulsion droplets can also be obtained with this method using another system.

Thus, allowing the scalable formation of anisotropic droplets of significantly different physicochemical properties and demonstrating that this mechanism may be applied to various systems.

2. Materials and Methods

2.1 Preparation of Anisotropic Emulsions

Unless otherwise stated all materials were used as received. 3 mL of dopamine hydrochloride (0.05 M, Alfa Aeser) was placed in a 20 mL vial followed by 100 µL of 18 mM of cetyltrimethylammonium bromide (CTAB, Panreac AppliChem). This solution was then mixed by shaking and 250 mg of hexadecane (Sigma) was added and emulsified via ultrasonic probe (Fischer FB505, 20 kHz, 500 W) for 1 min at 20% amplitude while the vial was immersed in a water bath at RT. A magnetic stirrer bar was added to the newly formed emulsion and allowed to stir for 30 min. Following this, 1.6 mL of tris(hydroxymethyl)aminomethane hydrochloride (Tris-HCl buffer, pH 8.5, Sigma) was added to the emulsion to both initiate polymerisation and accelerate coalescence. The emulsion was allowed to stir for 24 h before being centrifuged (Megafuge 16R, Thermo Scientific) at 4000 rpm for 20 min to separate emulsion droplets from free polydopamine (PDA) particles in the continuous phase (Figure 1, PDA/CTAB emulsion).

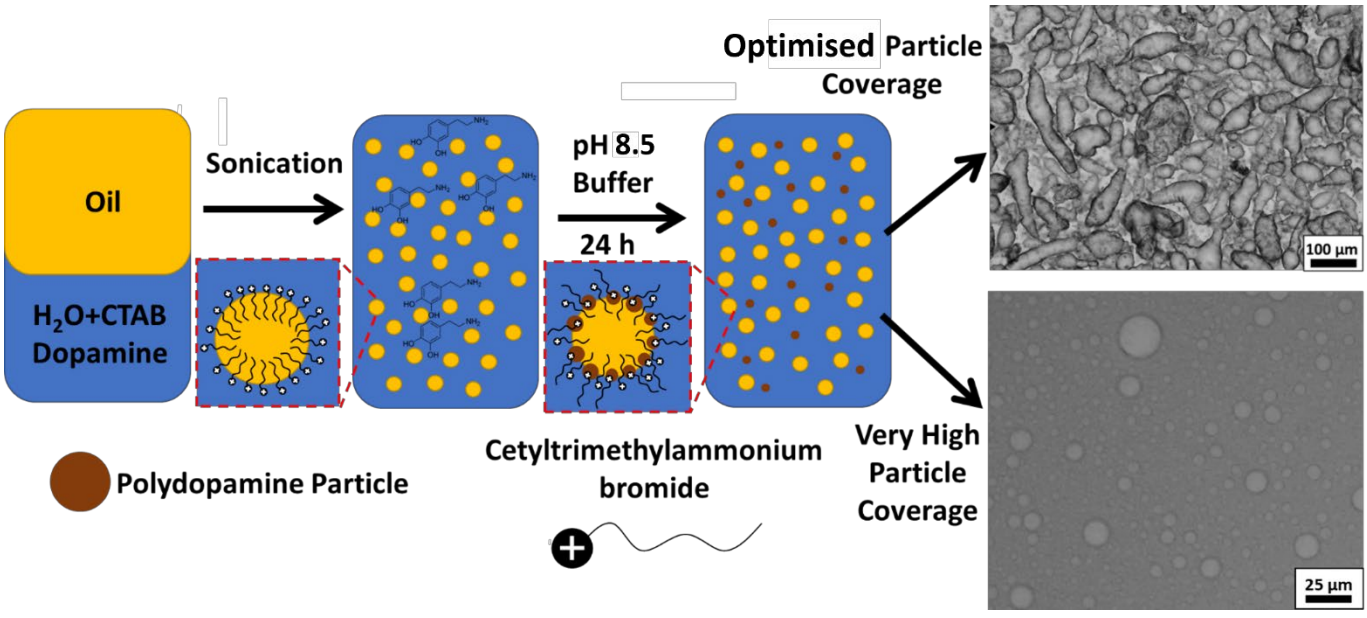

Figure 1. Schematic of anisotropic emulsion formation. Initial CTAB-stabilised emulsion formed with dopamine monomer present in the continuous phase. pH 8.5 buffer is added while stirring, thus inducing chemical oxidative polymerisation of dopamine and simultaneous electrostatically driven emulsion destabilisation (coalescence). Polydopamine particles are formed in the continuous phase, and stabilise the interface, while some oligomers also remain in the continuous phase, resulting in non-spherical emulsion droplets (right). An optimised ratio between the O/W interfacial area present in the system and the number of particles formed exist. If this ratio is too low (ie a higher concentration of dopamine is used), droplets are too well stabilised by the formed polydopamine particles and do not undergo the arrested coalescence process.

In order to demonstrate that this arrested coalescence mechanism leading to the production of non-spherical droplets was not exclusive to the dopamine/CTAB system, a second emulsion

system was tested where the monomer pyrrole (Py, Sigma) was used instead of dopamine. 3 mL of 1 mM solution of sodium dodecyl sulphate (SDS, Sigma) was combined with 250 mg of hexadecane and subjected to emulsification as outlined above. 160 mg of Py (which was purified via a basic alumina column (Brockman's I, Sigma) before addition) was added to the emulsion and allowed to stir for 1 h. Finally, 1.6 mL of 150 mM $H_2PtCl_6.xH_2O$ (Sigma) was then added to the emulsion before leaving the system to polymerise and coalesce while stirring for 7 days (Figure S1) based on previous work by Takeoka et. al [23]. Particles formed in the bulk were separated at the end of this process via centrifugation as outlined above.

2.2 Optical, Fluorescent & Cryogenic Scanning Electron Microscopy

Optical micrographs were obtained using an Olympus BX51 microscope with fluorescent light source (Olympus U-RFL-T). Hexadecane was spiked with Nile Red was used to monitor the presence of the oil throughout the process and verified that no significant phase separation had occurred. Confocal fluorescent images of the PPy-SDS emulsions were captured on a Zeiss LSM880. CryoSEM samples were prepared using a freezing rivet that was submerged in liquid nitrogen before being transferred under vacuum into a Quorum PP3010 cryo-preparation chamber. The sample was fractured using a cooled knife and allowed to sublime to reveal emulsion droplets beneath the ice layer. An Iridium coating was sputtered onto the samples, before being transferred into a Thermo scientific Helios G4 CX DualBeam operating at 2 kV. Cryo conditions were maintained throughout analysis.

2.3 Impact of Electrolyte Concentration

The effect of electrolyte concentration on the resultant emulsion shape was explored by varying the concentration of the Tris-HCl buffer (from 0 to 0.64 M) added to the emulsion while maintaining the same volume and pH of 8.5.

Emulsion droplet shape was evaluated using a FlowCam cytometer (C70 Benchtop, FluidImaging). The FlowCam was programmed to take images until 1M droplets were identified by the software in AutoImage mode using a 10x objective for most emulsions, and a 20x for the 0 M Tris-HCl sample due to its smaller size. A FC100x2 flow cell was used in a reverse flow configuration for these measurements due to the density difference between the oil and the continuous phase. Post capture, the droplet images were processed with VisualSpreadsheet native instrument software eliminating droplets out of focus using the edge gradient function. The anisotropy of the droplets was assessed using the circle fit software function (Further details in SI).

2.4 Impact of Shear Rate

To investigate the impact of shear rate on the shape and characteristics of the emulsions, additional emulsions were formed as outlined in §2.1 with all concentrations kept constant, but volumes increased by a factor of 10. Emulsions were also formed via sonication for 11 minutes instead of 1 minute in a 100 mL round bottomed flask to maintain the J/m^3 energy input into the system. This flask was then subjected to shear using an overhead stirrer with an impeller (IKA) for 24 h at 250, 375, and 500 rpm instead of using a magnetic stirrer. Samples were kept in a water bath 25 °C during sonication and polymerisation. Differences in size

distribution between these samples was investigated using laser diffraction (Malvern Mastersizer 3000) equipped with a hydro-dispersion unit (Hydro-MV) and sphericity measured using the Flowcam as outlined above.

2.5 Zeta Potential

An aqueous phase was prepared as outlined in §2.1 but without the addition of an oil phase or use of the ultrasonic probe, resulting in a PDA particle dispersion (PDA-AP). Briefly, a 3.1 mL solution containing 0.15 mmol of dopamine hydrochloride and 1.8 µmol CTAB was combined with 1.6 mL of Tris-HCl buffer (pH 8.5, 1M) in a 20 mL vial and allowed to polymerise for 24 h under magnetic stirring. Following this, a dialysed sample was prepared by placing the PDA dispersion in dialysis tubing (MWCO 8000 Da) and placed in a 2.5 L beaker of water. Water was then changed daily until conductivity and pH were the same as that of pure water to remove excess surfactant, buffer and, monomer and oligomer <8kDa (PDA-D). This sample was then used as the aqueous phase, before separate addition of Tris-HCl buffer (PDA-Tris) and CTAB (PDA-CTAB) and a combination of both (PDA-Tris/CTAB) to match the conditions used in initial particle/emulsion preparation. Zeta potential of the PDA particle systems was measured using a Malvern Zetasizer Ultra using a DTS1070 Malvern cell.

2.6 Interfacial Tension & Shear Rheology

Interfacial tension (IFT) for each particle dispersion described in §2.5 was also measured against a hexadecane oil phase. This was achieved using the pendent drop method [24, 25]. The bare water/hexadecane interface was measured prior to any additional measurements to ensure correct fitting and establish a baseline. In each case, the aqueous phase was injected into the oil phase until the characteristic pendent droplet was able to form due to the force balance γ_{AO} and gravitational forces. The Young-Laplace equation was then fitted to the droplet by the native instrument software to determine γ_{AO} [24, 26].

Interfacial shear rheology (IFSR) was also performed using PDA-AP and PDA-Tris/CTAB using a hexadecane oil phase for comparison (Discovery HR-2, with double wall ring geometry). The base receptacle was first filled with 19.3 mL of aqueous phase, and the ring lowered to be in contact. The ring was then lowered until half the ring was covered, and hexadecane added to the receptacle to form an o/w interface. Initial studies were performed to measure the elastic/storage (G') and viscous/loss modulus (G'') at a 1% strain and 0.5 Hz oscillation rate for 1 h. Following this, the samples were subjected to a strain amplitude sweep from 0.01 to 100% to investigate the yield strain of the formed films.

3. Results & Discussion

3.1 Preparation of Anisotropic Emulsions

Micrographs reveal the presence of a large number of non-spherical droplets in the PDA/CTAB emulsion (Figures 1 & 2). Furthermore, the use of CryoSEM allowed for visual inspection of the surface of the emulsion droplets. These emulsion droplets appear to be armoured with particles of various sizes and exhibit a high aspect ellipsoid shape characteristic of an arrested coalescence phenomenon [16-18, 27]. In this case, the base emulsion is stabilised by ionic surfactants, where a repulsion based on electrostatic interactions provided by the surfactant

generates this stabilisation and is governed by classic DLVO theory [28, 29]. Briefly, DLVO theory delineates the stability of dispersed systems as a balance between repulsive electrostatic interactions and attractive van der Waals forces. The range of the electrostatic repulsive force is defined by the Debye Length (κ^{-1}),

$$\kappa^{-1} = \sqrt{\frac{k_B \varepsilon_0 \varepsilon_r T}{e^2 \sum_i z_i^2 n_i}} \qquad (2)$$

where k_B is the Boltzmann constant, $\varepsilon_0\varepsilon_r$ is the product of the vacuum permittivity and relative permittivity of the medium, T is the temperature, e is the charge on an electron, n is the number density of ion species (i) and valence z. It is important to note, that this electrostatic repulsive range decreases as a function of the increase in electrolyte concentration as the surface charge on the droplet becomes increasingly screened, thus accelerating coalescence in the emulsion. In this case, the reduction in Debye length and resultant increased coalescence is initiated by addition of relatively concentrated electrolyte (Tris-HCl). Simultaneously, the electrolyte results in the chemical oxidative polymerisation of dopamine to polydopamine, forming PDA particles in the bulk and in the continuous phase [30, 31]. These polymer particles may then electrostatically interact with the surfactant, increasing their surface activity and driving increased droplet surface coverage with time. Specifically, the negatively charged catechol group present in PDA is likely to interact with the cationic head group of CTAB [32].

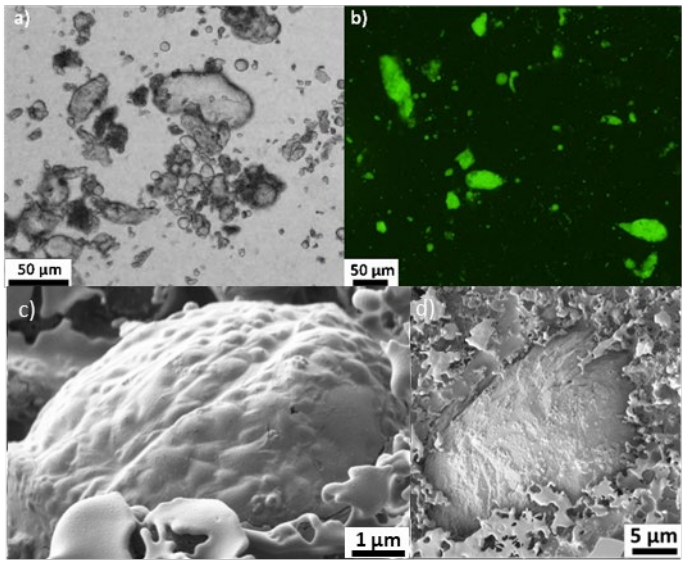

Figure 2. Micrographs of PDA/CTAB non-spherical emulsions. a) Optical micrograph of emulsion formed with electrolyte concentration of 0.32 M. b) Repeated emulsion stained with Nile Red under fluorescence. (c,d) CryoSEM micrographs of emulsion droplets for a sample prepared using 0.32 M Tris-HCl.

This complementary particle/surfactant interaction is reported throughout the literature for a number of particle/surfactant combinations [33-37]. As a result of these interactions, the particles are driven to the oil-water interface present in the system and thus contribute to the stabilisation of the corresponding emulsion droplets. In summary, while the interfacial area of the emulsion decreases with time due to coalescence, the concentration of effective emulsifier present in the system increases. Consequently, as the stabilising PDA particles are

irreversibly adsorbed at the interface as outlined above (Equation 1), the particles become jammed at the interface and resist the interfacial tension driving the coarsening and sphericity of the droplets. This results in the observed morphological anisotropy. Indeed, this process is a kinetic balance between the electrolyte-induced coalescence of the surfactant stabilised emulsion and the formation and adsorption of the polymer particles. Pawar et al reported that for a two-droplet coalescence event, when combined fractional particle interfacial coverage was above 0.9 no coalescence was possible, and below 0.7 complete coalescence occurs, and only between these two coverages can arrested coalescence take place [17]. Thus, if coalescence is too slow, more particles are able to stabilise the droplets and coalescence is subsequently inhibited. Conversely, if coalescence is too fast then insufficient coverage occurs, thus resulting in complete coalescence. We monitored the kinetics of both PDA polymerisation and the destabilisation of the CTAB emulsion and the, which are presented in Supporting Information (Figures S2 – S6. Polymerisation kinetics were followed by NMR spectroscopy using the disappearance of the dopamine monomer peak over time [38]. These results showed that over 20% of the monomer is consumed 2h after addition of the Tris buffer, which starts the polymerisation reaction. After 8h, 60% of the monomer was used in the polymerisation, which appeared to be complete after 24h (with no monomer detected in the system by that point Figures S2 – S5). These data can be compared to those obtained when monitoring the emulsion droplet size increase over time, which is indicative of the coalescence kinetics (Figure S6). On similar time scales, between 3-5 h after buffer addition, the emulsion droplet size distribution begins to broaden, and shifts to larger sizes. This is an important observation as if the polymerisation and coalescence kinetics were not comparable, (i.e. polymerisation or coalescence was too fast/slow) then arrested coalescence would not take place. Specifically, if droplets completely coalesce before particle formation, then only spherical large droplets would result from this process. Inversely, if particles fully form before droplet coalescence occurs, the process would lead to small spherical particle-stabilised emulsions (Figure 1).

Furthermore, CryoSEM images (Figures 2c-d) and associated EDX elemental mapping (Figure S7) indicate that the droplets are indeed covered with a film in which discrete particles appear to be embedded. This is concordant with the proposed formation mechanism of initial particle stabilised emulsion formation reinforced by a polymeric film. In addition, the CryoSEM images demonstrate that despite the non-sphericity being driven by coalescence of smaller droplets, and primarily resulting in large droplets (length >50 μm), smaller (length of ~10 μm) non-spherical droplets are also still present in the sample, likely as a result of small droplets with a high polydopamine particle coverage coalescing together into an arrested shape.

3.2 Impact of Electrolyte

The primary emulsion is electrostatically stabilised by the cationic surfactant CTAB as outlined by basic DLVO theory. This emulsion consists of droplets of approximately 1 μm diameter and is stable to coalescence and creaming (Figure 3 and Figure S6). Upon addition of the electrolyte, which initiated the polymerisation and accelerated coalescence, the droplets start increasing in size and become more non-spherical. The extent of this coalescence and droplet anisotropy is proportional to the concentration of electrolyte in the aqueous phase

and the consequent extent of screening of the electrostatic-driven repulsion generated by the CTAB adsorbed on the droplet surfaces (Figure 3). It is not expected that the increase in buffer concentration will substantially affect the polymerisation kinetics as they are primarily first order with respect to dopamine monomer concentration [39]. In addition to the increase in size and anisotropy, the droplets appear to become covered by an interfacial film as the electrolyte concentration increases which becomes visibly coarser both over time and proportionately to electrolyte concentration. The presence of this film is especially apparent when comparing the samples prepared with 0.08 M and 0.48M Tris-HCl concentrations. These findings are directly comparable to those reported by Tyowua et. al. who produced non-spherical emulsions by preparing Pickering emulsions stabilised by $CaCO_3$ in varying NaCl concentrations [40]. They proposed that electrostatic stabilisation was achieved by interparticle repulsion between the adsorbed $CaCO_3$ particles and only occurred at certain salt concentration ranges. However, the method reported herein relies on in-situ generation of the particulate stabiliser and a synergistic effect of the forming particles and surfactant at the oil/water interface during coalescence. Furthermore, here the initial emulsion droplets are small (< 1μm), as a result of their stabilisation with a surfactant instead of large particles, thus resulting in micron-sized non-spherical emulsion droplets at the end of the polymerisation/coalescence process.

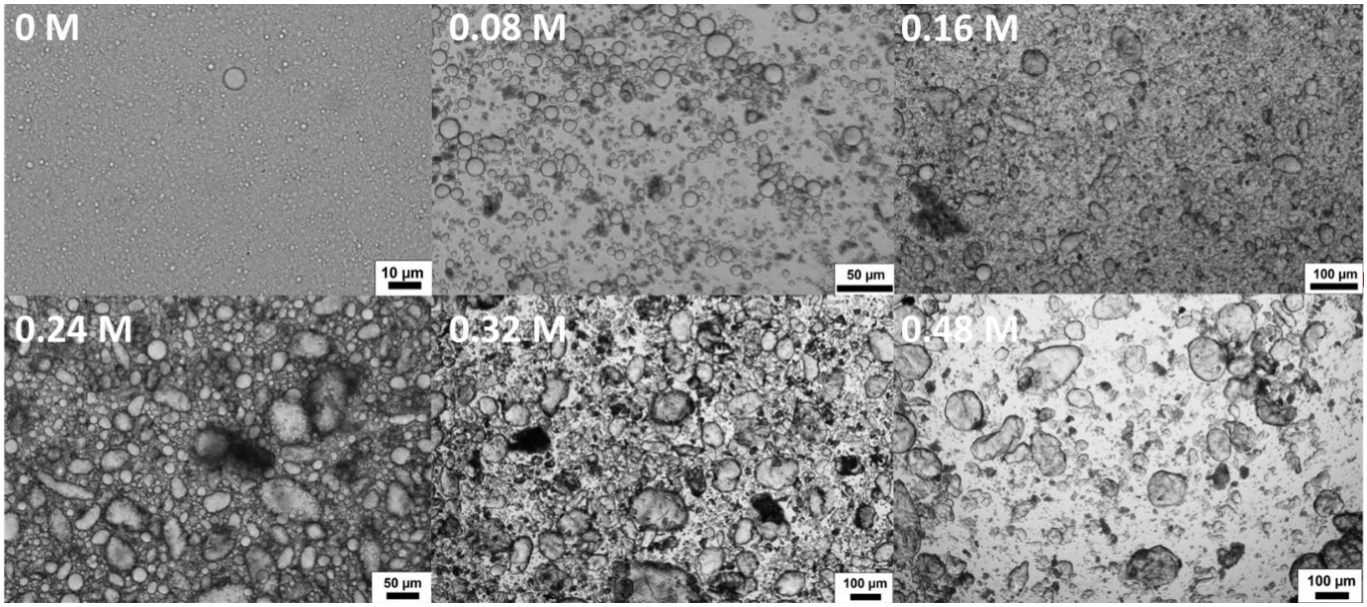

Figure 3. Micrographs of PDA/CTAB emulsion formed by increasing final electrolyte concentration. Concentrations in each image correspond to final Tris-HCl concentration during coalescence.

Emulsion droplet characteristics analysis in a flow cell (using a Flowcam instrument - Figure 4) confirmed the qualitative observations made above for emulsions processed with increasing Tris-HCl concentration. The circle fit function was chosen to quantify the anisotropy of the imaged emulsion droplets, which measures the deviation of the captured droplet profile from that of a projected circle. The inset in Figure 4 presents examples of droplets of increasing circle fit from 0.1 to 1, where 1 represents a perfect sphere and 0.1 the largest deviation from a circle. Based on these images, and the circle fit distribution of the CTAB-stabilised emulsion (Figure 4), droplets were characterised as either being spherical (circle fit ≥0.9) or non-spherical (circle fit ≤0.8). As expected, when there was no added Tris-HCl, the

emulsion was almost completely spherical. However, on addition of the electrolyte, this circle fit decreased as the emulsion evolved from a surfactant-stabilised emulsion to one where the oil-water interface is stabilised by both particles and surfactant while undergoing coalescence. When an increasing concentration of Tris-HCl was used to polymerise and destabilise the emulsion, the degree of anisotropy slowly increased. This reached a maximum within the range tested at 78% of droplets being non-spherical (Figure 4).

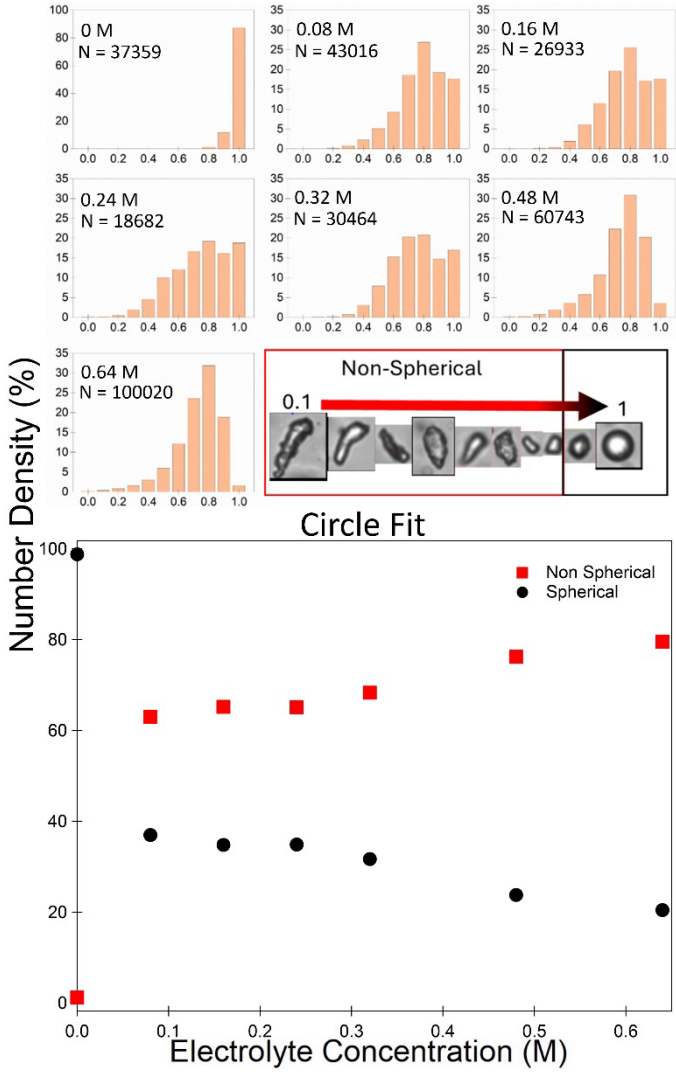

Figure 4. a) Number percentage of spherical and non-spherical droplets as a function of increasing electrolyte concentration during emulsion preparation for PDA/CTAB emulsions. Top: full distributions of circle fit measurements performed using FlowCam and number of droplets measured (N). The 0 M sample represents a sample that is not destablised and was used to classify droplets as being spherical or non-spherical. Droplets are classified as being spherical if circle fit was ≥0.9 as indicated by the inset in the top figure. Inset provides examples of droplets of increasing circularity and examples of image quality obtained from the FlowCam analysis of droplets for each electrolyte concentration including at least 2 repeats of each condition. Bottom: Cumulative number density of particles being classified as spherical or non-spherical as outlined above as a function of electrolyte concentration.

This is once more concordant with the proposed mechanism of an arrested coalescence phenomenon. As the emulsion quickly coalesces, the droplets become increasingly larger, and

as outlined above, the total interfacial area decreases until it can no longer support the number of polymeric particles adsorbed at the interface. As a result, the larger droplets are more likely to result in arrested coalescence, and a higher aspect ratio [16, 18, 40, 41].

3.3 Impact of Shear Rate

By using an overhead impeller, it was possible to maintain the same geometry while increasing the shear applied during the coalescence and polymerisation process. Optical micrographs of the emulsions at increasing impeller rotation speed (Figure 5a) reveal that, particles appear to form a thicker PDA interfacial film at lower shear, resulting in opaque droplets. As the shear rate increases (375 RPM), the droplets exhibit thinner particle shells, and there appears to be a larger number of smaller droplets or particles dispersed in the continuous phase. When examining the sample prepared at the highest shear tested (500 RPM), highly deformed emulsion droplets with an apparently thinner PDA interfacial film can be observed. On measurement of the droplet morphology using the FlowCam, (Figure 5b) the increase in impeller RPM appears to result in an increased number of spherical droplets. However, for the same Tris-HCl concentration as the data presented in Figure 4a, the overall number of non-spherical droplets is higher at low RPM but lower at higher RPM.

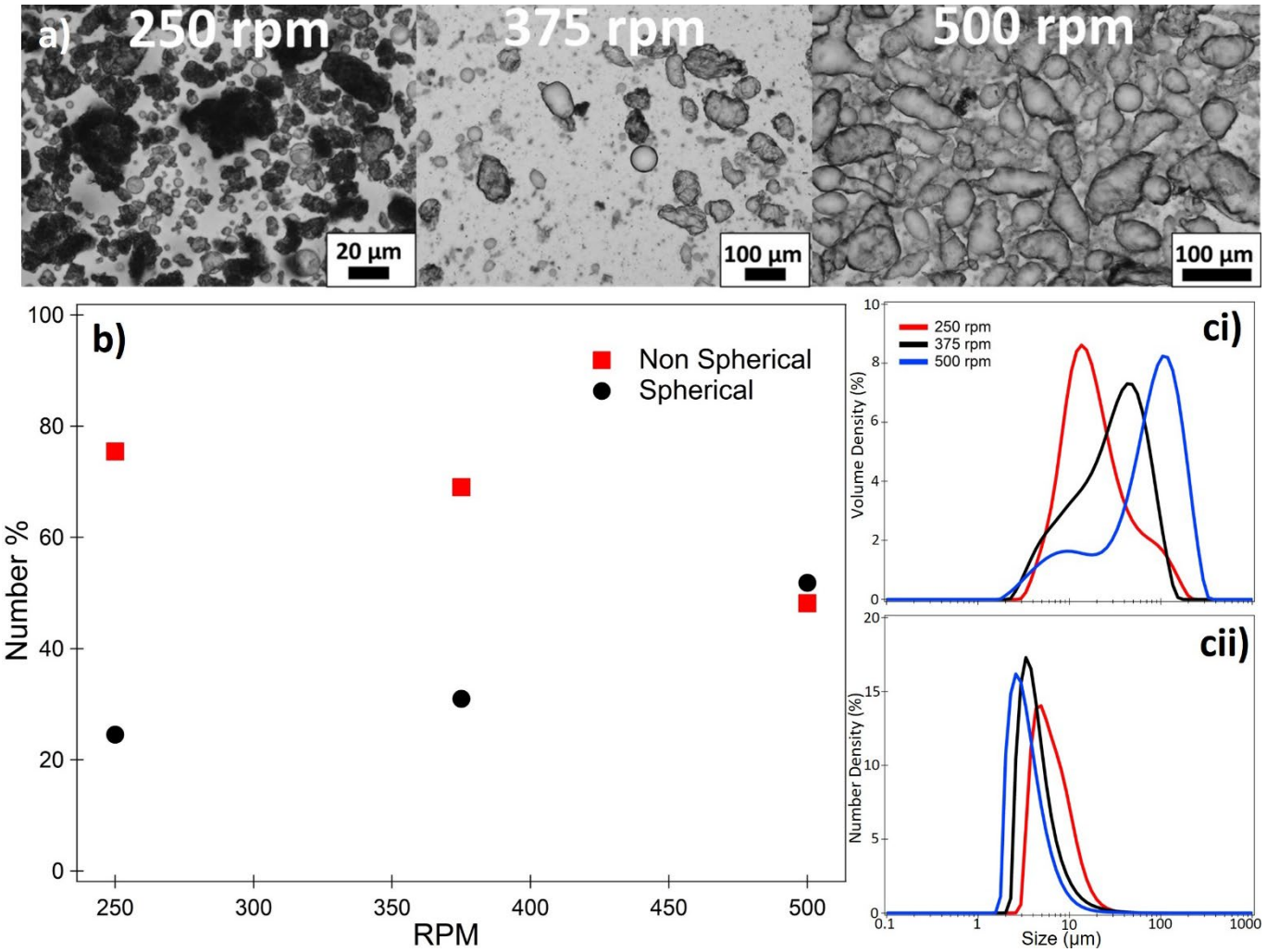

Figure 5. Impact of stirrer rotation speed (shear rate) during emulsion preparation on size and anisotropy of PDA/CTAB formed emulsion droplets at a Tris-HCl concentration of 0.32 M. (a) Optical

micrographs at increasing shear rate. (b) Number percentage of spherical and non-spherical droplets as outlined in Figure 4 as a function of increasing shear rate. (ci) Laser diffraction determined size distribution (volume %) and number % (cii) As a function of shear rate.

The use of an overhead impeller not only ensures more uniform mixing when compared to a magnetic stirrer, but also results in an increased overall shear stress applied to the emulsion system. As a result, the increase in initial droplet anisotropy observed in Fig 5b when compared to Figure 4 can be explained via deformation of the emulsion droplets due to the applied shear field [42, 43]. This may seem counterintuitive, as at increasing RPM the droplets tend to become more spherical (by number), contradicting the micrographs. However, as the shear rate increases, two competing phenomena begin to occur. The shear accelerates coalescence in the droplets resulting in the shift of the volume distribution presented in Fig 5ci [44]. However, on examination of the number distribution (Figure 5cii), the opposite appears to be the case as the peak begins to shift to a smaller diameter as the impeller RPM is increased resulting in an increase in D[4,3], D[3,2] (albeit at a smaller rate) and Dv50, while Dn50 decreases (Table 1). This is likely due to the high shear stress not only deforming the emulsions as outlined above, but also further breaking them into smaller secondary droplets [43]. These droplets, having not undergone the same initial coalescence/polymerisation process likely become quickly stabilised by particles in the bulk, but also any remaining surfactant, and as a result, remain spherical by the end of our process. These results can be related to work carried out by Whitby et al, who reported that at sufficiently high shear, not only do Pickering emulsion undergo coalescence, but that particles adsorbed at the interface may also become dislodged by the shear and returned to the bulk [44]. In such a case, these particles would then be available to stabilise the aforementioned secondary droplets, resulting in the increased occurrence of spherical droplets, or particle flocs. These simultaneous processes are concordant with the findings in Figure 6, where the detachment of particles and deformation at high shear would result in high aspect ratio droplets possessing thinner films, while the presence of such particles and droplets would decrease the median number distribution while simultaneously increasing the volume average and sphericity.

Table 1. Droplet diameters of PDA/CTAB anisotropic emulsions prepared at increasing stirring rates during coalescence and polymerisation determined by laser diffraction. It is important to note that due to the nature of the Mastersizer measurements (assumption of spheroid particles) the exact numbers presented may not be reflective of the true particle size. However, the general trends and shifts of the distribution are still valid.

Stirring Rate (RPM)	D[4,3] (µm) Determined by Laser Diffraction	D[3,2] (µm) Determined by Laser Diffraction	Dn50 (µm) Determined by Laser Diffraction	Dv50 (µm) Determined by Laser Diffraction
250	27	18	5	24
375	34	22	6	31
500	97	32	3	88

3.4 Zeta Potential

PDA particles were separately prepared in an aqueous phase (in the absence of an oil phase) as outlined in §2.5 and the system was dialysed to ensure only the particles were present in the suspension. The zeta potential of this PDA particle suspension was then measured in pure water and when Tris-HCl buffer and CTAB surfactant is added to the dispersion (Table 1). Interestingly, despite monomer not being present after 24 h of polymerisation (Figures S5 &

S7), the dialysis medium would begin increase in opacity over time, and nanoparticles could be measured using dynamic light scattering (Figure S8).

Table 2. Zeta potentials of PDA particles before and after dialysis and addition of surfactant and buffer at identical concentrations to emulsions

Sample	**pH**	**Zeta Potential**
PDA-AP	8.5	-30 ± 1
PDA-D	6.7	-19 ± 0.4
PDA-CTAB	6.2	33 ± 2
PDA-TRIS	8.6	-38 ± 0.2
PDA-CTAB/TRIS	8.6	39 ± 1

The polydopamine particles prepared under the same conditions as the emulsions (without oil, PDA-AP) presented with a negative potential at the threshold of dispersion stability (-30 mV). This is in contrast to the dialysed sample (PDA-D), which has a slightly less negative potential, likely due to the change in pH between water and the Tris buffer. However, once dialysed and the same amount of Tris buffer is re-added to the suspension (PDA-TRIS), the zeta potential becomes significantly more negative. This is likely because the PDA-AP sample contains more electrolyte overall and thus its particle charge is diminished through charge-screening. Conversely, the samples where CTAB is present show a positive zeta potential demonstrating strong interaction between the surfactant and the PDA particle surface, which initially is negatively charged. This polarity flip is characteristic of a bilayer of CTAB molecules assembling on the particle surface [34, 45]. Initially the cationic head group interacts with the anionic polymer particle, resulting in a net reduction in particle charge, however on further addition of CTAB, tail-tail interactions result in the slipping plane becoming positive due to the formation of micelles or admicelles on the solid surface [34, 45]. It is possible that, in the PDA-AP sample, the surfactant is electrostatically interacting with dissolved monomer or oligomer in the bulk and is incorporated into the particle, rather than adsorbed at the surface, resulting in the negative zeta potential. Previous studies have reported that the presence of ionic surfactants can impact the polymerisation and affect PDA film deposition [46, 47]. These oligomer/surfactant interactions appear to have significant implications on the film formation described above and are further investigated below.

3.5 Interfacial Tension & Shear Rheology

As mentioned above, the PDA particles forming during the polymerisation process appear to form a strong film on the droplet surface, leading to prolonged resistance to coalescence after the polymerisation/coalescence process is complete. Thus, interfacial tension measurements were undertaken to investigate this film and the impact of each of the other components of the system. When using the PDA-AP particle suspension only, the droplets formed in hexadecane initially appeared to adopt the traditional pendent shape (Figure 6a). However, after approximately 400 s, a film became visible at the interface. At this point the Laplacian fit employed by the instrument software was unable to accurately fit the droplet, which no longer possessed a pendent shape [48]. When left to age for several hours, the film thickened

and began to deform under the weight of the internalised liquid (Figure 6b). This indicated the strong adsorption of particles at the liquid/liquid interface and the formation of an elastic shell. Often in such experiments, this typical elastic shell is only visible upon droplet compression, but spontaneous wrinkling in this case suggests that additional interactions are reinforcing the interfacial particle network – potentially crosslinking by the aforementioned dissolved PDA polymer or oligomers [21, 49].

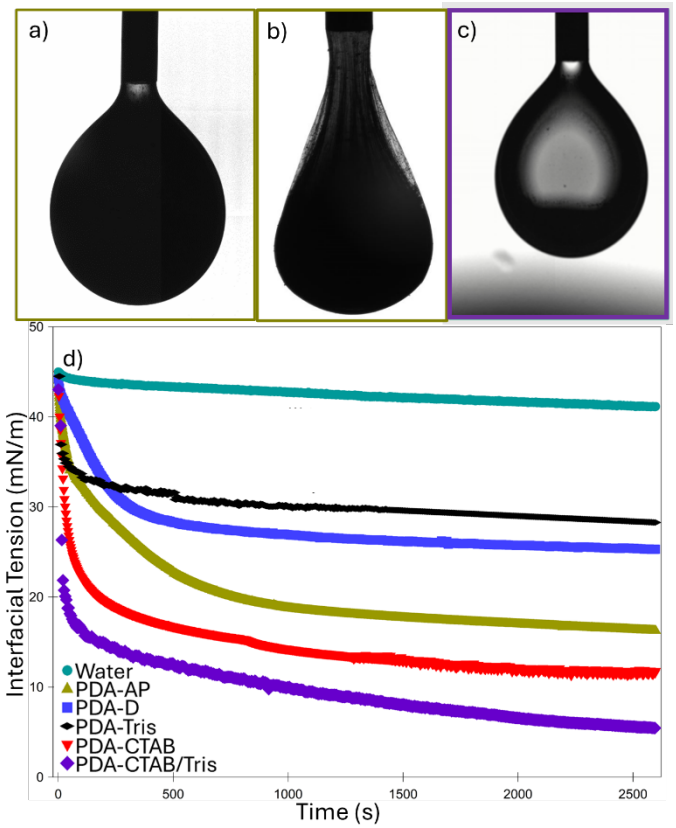

Figure 6. Pendent drop tensiometry of polydopamine particles dispersed in an aqueous phase suspended in a hexadecane oil phase. (a) Photograph of polydopamine particle dispersion as prepared in the emulsion (PDA-AP) at time 0 immediately after suspension in oil. (b) after 2 h demonstrating viscoelastic film formation. It is important to note, that no aqueous phase was withdrawn for this film to be visible. (c) Photograph of dialysed polydopamine particles after addition of CTAB and 0.34 M Tris-HCl (PDA-CTAB/Tris) after 1h (no film apparent). (d) Interfacial tension data of aqueous droplets formed in hexadecane for pure water, PDA-AP suspension, dialysed polydopamine particle (PDA-D) suspension, dialysed polydopamine particles dispersed in 0.34 M Tris-HCl (PDA-Tris), dialysed particles in 0.4 mM CTAB (PDA-CTAB) and PDA-CTAB/Tris. Videos available in supporting information.

This hypothesis is further supported by examination of CryoSEM images in Figure 2c-d where particles are clearly seen to be embedded in a film, rather than organised discretely at the interface. Furthermore, the interfacial tension measurement of the PDA suspension with CTAB and Tris added, (Figure 6c) which had been prepared at the same CTAB and Tris-HCl concentration as PDA-AP and the emulsion post dialysis, exhibits extremely different behaviour. No film is visible in these experiments, and the interfacial tension (Figure 6d) is observed to drop at a much faster rate, characteristic of surfactant adsorption rather than

particle adsorption. Indeed, on retraction of the droplet, no buckling or deformation was observed, indicating either the lack of, or weakly adsorbed particles at that O/W interface. Similarly, the PDA-CTAB demonstrates very similar behaviour, but is slightly less effective at reducing the interfacial tension, potentially due to the Tris-HCl screening electrostatic repulsion between the charged CTAB head groups at the interface, thus resulting in a higher surfactant coverage [50]. This contrasts with the PDA-Tris sample which showed the least interfacial activity. Visually, a pendent droplet was visually formed, however the interfacial tension measurement exhibited unusual behaviour. The IFT appeared to decrease relatively quickly but the total change in interfacial tension was minimal (only 10mN/m). It is likely that these particles were simply not sufficiently surface-active owing to the increase in pH provided by the Tris-HCl and consequent surface charge. Indeed, this is in agreement with the large zeta potential of these particles measured in Table 2 However, when adding Tris to the initially dialysed sample, it is possible that some aggregates formed during dialysis and remained in the suspension. As a result, these aggregates would quickly sediment, deforming the droplet, which is misinterpreted by the software as a decrease in IFT [51]. Finally, the dialysed PDA particles appear to be able to lower the interfacial tension in their native state likely due to the pH of the Milli Q water being around 6.5 – similar to the first average pKa of PDA due to the quinone-imine moieties [52]. However, the catechol groups are still protonated, resulting in a diminished charge and increased amphiphilicity (Table 2), when compared to the other samples which after Tris-HCl addition are at pH 8.5 (close to pka of the PDA catechol groups – 8.9) [52]. At which point significant deprotonation will take place resulting in an increased negative charge. Indeed, dialysed PDA was able to demonstrate film wrinkling on droplet volume reduction (Video SX) and is reported to be sufficiently surface active to stabilise an emulsion [53].

Interfacial Shear Rheology (IFSR) measurements allowed for the monitoring of film formation in-situ. The storage (or elastic) modulus G', and loss (or viscous) modulus G'' were studied for all the PDA samples investigated with the interfacial tension measurements, however only PDA-AP and PDA-D presented a G'. This indicated that particles that only samples PDA-AP and PDA-D offered a rheological response characteristics of particle films. The response provided by all the other samples was instead characteristic of surfactant stabilised interfaces, which possess only Gibbs elasticity [54]. These findings were also concordant with the behaviour described in discussion of the interfacial tension measurements in Figure 6 and the larger positive zeta potential described in §3.4. IFSR was also used to investigate the impact of PDA-AP concentration on film formation behaviour (Figure 7). For both concentrations of PDA-AP studied, G'' initially dominates indicating that the interface is acting as a fluid and flows under the applied strain [55-57]. However, over time the G' increases and reaches a characteristic cross-over point with G'' for transitioning to an elastic interface likely due to an increasing number of particles adsorb at the interface [58-60]. At this point, the interface no longer flows like a liquid as interparticle, and particle-interface interactions begin to dominate. Beyond the cross-over point, G' continues to increase over time, eventually reaching a maximum. A strain sweep was performed on each of the samples after being allowed to form for 2 h. For samples studied at low shear stress (strain <2%), the interfacial moduli were independent of applied strain, indicative of a linear viscoelastic region dominated by the solid-like behaviour of the

PDA-AP film. However, at a critical strain, G' begins to decrease and crosses over with G'' as the interface begins to yield and flow like a fluid [56]. Comparing the behaviour of the different concentrations of PDA-AP, it can be seen from Figure 7 that the critical strain required to force the particle-laden interface to yield increases as a function of PDA-AP concentration. Furthermore, the time taken for G' to become dominant increases as the concentration of the particles is decreased. This indicates that the time taken for the elastic film to form is, as can be expected, inversely proportional to the concentration of particles present in the aqueous phase, while the yield strain is proportional after initial film formation.

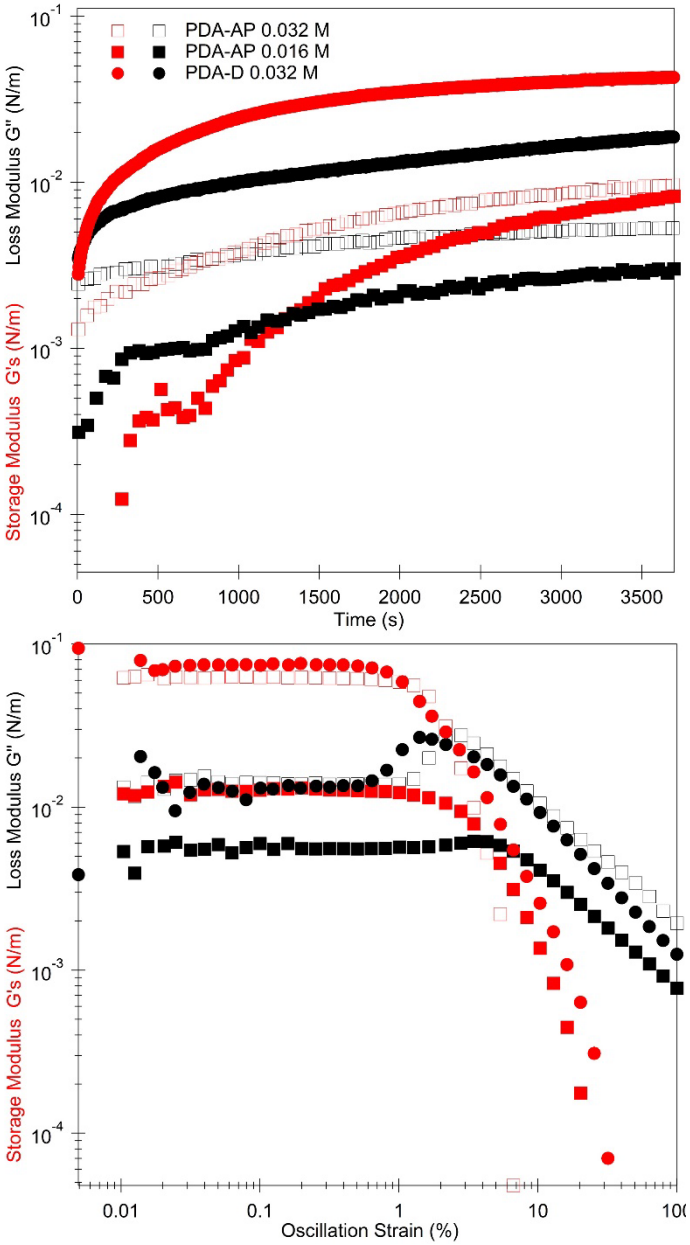

Figure 7. Interfacial properties of PDA/CTAB – hexadecane film. Top: Oscillatory measurements performed on film at 0.5 Hz at a strain amplitude of 1% for PDA-AP at 0.032

M and 0.016 M nominal concentration. Bottom: Strain amplitude measurements performed on film after oscillatory measurements (2 h).

3.6 Polypyrrole/SDS Emulsions

In order to demonstrate that this phenomenon is not restricted to a single combination of the stabilisers, a second system was explored. Pyrrole can be readily polymerised into polypyrrole in a number of ways notably using $FeCl_3$ and metal salts, The metals in this case oxidising the pyrrole monomer, and being reduced to $FeCl_2$ and Pt nanoparticles in the process [23, 61, 62]. In this case we chose to use chloroplatinic acid which allows for formation of polypyrrole through chemical oxidative polymerisation. In this system, the polypyrrole polymer forms both at the interface and in the water phase, owing to partitioning of the pyrrole monomer in both phases as it has some solubility in both (LogP 0.8). In the aqueous phase, the polypyrrole polymer is insoluble and thus precipitates into particles, which can contain platinum nanoparticles within them as a result of the corresponding reduction reaction induced by the choloroplatinic acid reacting. Here we refer to these particles as PPy-Pt [23, 63].

This process can be compared to that above for the PDA/CTAB system as, in this case, the metal salt both induces an increased coalescence rate of the emulsion initially stabilised by SDS and initiates the polymerisation and PPy-Pt particle formation. Figure 8a-b reveals the presence of a large number of non-spherical droplets in this system resulting from 7 days of coalescence and polymerisation. The fundamental mechanism of arrested coalescence here is the same as that described for the PDA system, relying on particle formation and interaction with surfactant. Specifically, the positively charged amine of the PPy may interact with the anionic SDS (PPy-Pt/SDS) [64, 65]. The key difference is between these two systems is found in the longer polymerisation time of pyrrole, as well as the partitioning of the pyrrole monomer in both phases, resulting in direct polymerisation at the interface as well as in the bulk. This likely explains the slightly smoother appearance of the PPy-Pt/SDS emulsions seen in Figure 8a-d with clearly fewer discrete particles observed at the interface. When characterising the PPy-Pt/SDS emulsion at the end of the process, it was found that the sample also exhibits significant non-sphericity (Figure 8d). An interesting consequence of this formulation process is the potential to use further exploit the presence of the Pt nanoparticles. These nanoparticles could potentially be used for reaction catalysis or further encapsulation processes using these anisotropic emulsions as a template [66, 67]. The circle fit distribution of the PPy-Pt/SDS emulsion shows a large number of droplets (47%) in the 0.7 and 0.8 bins (non-spherical), and only 20% of the droplets are being measured as spherical (≥0.8). However, these systems were not as varied in their interfacial behaviour and are presented in Figure S9. PPy and PPy-Pt exhibited nearly identical, with only a small increase in interfacial tension reduction on the addition of SDS.

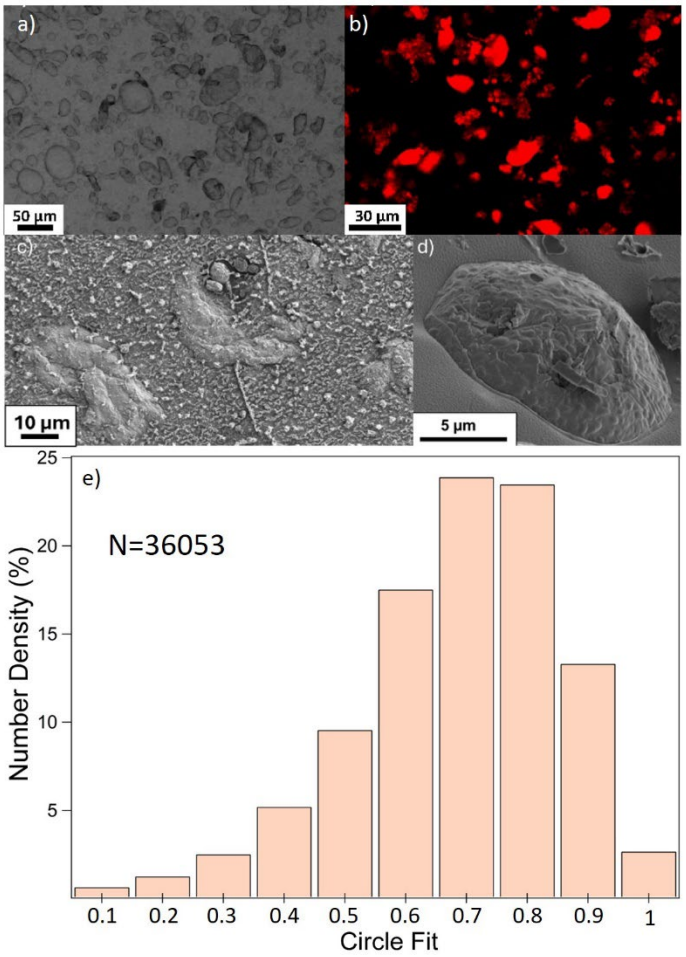

Figure 8. Micrographs and circle fit analysis of non-spherical PPy-Pt/SDS emulsions prepared using 150 mM H_2PtCl_6. a) optical micrograph emulsion. b) Repeated emulsion stained with Nile Red under fluorescence. c,d) CryoSEM micrographs of non-spherical emulsions. e) Circle fit distribution, where N is the number of droplets analysed.

4 Conclusion

Non-spherical oil/water emulsions were formed using a simple batch process via a simultaneous process of emulsion destabilisation and in-situ polymeric particle synthesis. The mechanism leading to non-spherical emulsion droplet shapes was demonstrated for two separate systems and could be achieved when monomer was present in either the aqueous (dopamine) or oil phase (pyrrole), using either cationic (CTAB) or anionic (SDS) surfactant, respectively. The extent of destabilisation, and degree of non-sphericity was proportional to the concentration of electrolyte added to the emulsion. At electrolyte concentrations of 80 – 640 mM Tris-HCl in the dopamine system, the number of non-spherical droplets was measured to be 60 – 80% by number, respectively. Retention of the oil was verified by detection of Nile Red dye within the emulsified hexadecane core. Shear rate was also found to be a significant factor in the formation of non-spherical emulsions. At lower shear rates (250 rpm) there was a high degree of anisotropy, and visibly larger interfacial coverage, while at higher shear rates (500 rpm) the number of spherical droplets in the resulting sample

increased. This was attributed to higher shear rates allowing for deformation of the droplets and increased collisions resulting in larger droplets by volume. However, this high shear was also capable of forming daughter droplets, which were inherently spherical, resulting in an increase in the number incidence of sphericity, as confirmed through laser diffraction. Finally, we investigated the interfacial behaviour of the stabilising particles using pendent drop tensiometry and interfacial shear rheology. Dialysed polydopamine particles exhibited some interfacial activity, concordant with existing literature, however on addition of the electrolyte buffer, this activity became diminished. On addition of CTAB to this system the interfacial activity appeared to be dominated by the surfactant indicated by the fast reduction in interfacial tension. These observations contrasted the observed behaviour of particles prepared in a similar manner to those stabilising the emulsion in the real system, which exhibited a reduced impact of the surfactant, followed by particle adsorption at the interface. However, the measurements of this particular sample may not be reliable due to the formation of a thick viscoelastic film, not adhering to a Laplacian morphology. This viscoelastic film was studied using interfacial shear rheology and the rate of film formation was found to be dependent on the ratio of stabilising polymer and oil/water interfacial area. Once formed, the magnitude of the elastic modulus was also dependent on the concentration of the particles present. This work offers the potential to form non-spherical polymer stabilised droplets using a simple scalable process, which may provide the possibility for increased efficiency in emulsion processing or may act as a template for non-spherical capsules, ideal for increased adhesion in a number of industrial setting such as washing/detergent and agrochemical applications.

Declaration of Competing Interest

The authors declare that they have no known competing financial interests or personal relationships that could have appeared to influence the work reported in this paper.

Data availability

Data will be made available on request.

Acknowledgements

The authors would like to acknowledge the financial support from the Engineering and Physical Sciences Research Council (EP/V027646/1, EP/V027654/1, EP/V027727/1). We would also like to thank Mr. Stuart Micklethwaite from LEMAS for technical assistance and sample preparation for CryoSEM imaging, Dr Jiatong Jiang and A/Prof David Harbottle for training on the IFSR and Dr Stephen Knox for training on benchtop NMR.

Appendix A. Supporting Information

References

[1] H.A. Jerri, M. Jacquemond, C. Hansen, L. Ouali, P. Erni, “Suction Caps”: Designing Anisotropic Core/Shell Microcapsules with Controlled Membrane Mechanics and Substrate Affinity, Advanced Functional Materials, 26 (2016) 6224-6237.

[2] A. Dong, Y. Wang, D. Wang, W. Yang, Y. Zhang, N. Ren, Z. Gao, Y. Tang, Fabrication of hollow zeolite microcapsules with tailored shapes and functionalized interiors, Microporous and Mesoporous Materials, 64 (2003) 69-81.
[3] K.M. Bromley, C.E. MacPhee, BslA-stabilized emulsion droplets with designed microstructure, Interface Focus, 7 (2017) 20160124.
[4] V. Kudryavtseva, S. Boi, J. Read, R. Guillemet, J. Zhang, A. Udalov, E. Shesterikov, S. Tverdokhlebov, L. Pastorino, D.J. Gould, G.B. Sukhorukov, Biodegradable Defined Shaped Printed Polymer Microcapsules for Drug Delivery, ACS Appl Mater Interfaces, 13 (2021) 2371-2381.
[5] V. Kudryavtseva, A. Bukatin, E. Vyacheslavova, D. Gould, G.B. Sukhorukov, Printed asymmetric microcapsules: Facile loading and multiple stimuli-responsiveness, Biomater Adv, 136 (2022) 212762.
[6] A.M. Bago Rodriguez, B.P. Binks, Capsules from Pickering emulsion templates, Current Opinion in Colloid & Interface Science, 44 (2019) 107-129.
[7] M. Gulumian, C. Andraos, A. Afantitis, T. Puzyn, N.J. Coville, Importance of Surface Topography in Both Biological Activity and Catalysis of Nanomaterials: Can Catalysis by Design Guide Safe by Design?, Int J Mol Sci, 22 (2021).
[8] M. Cooley, A. Sarode, M. Hoore, D.A. Fedosov, S. Mitragotri, A. Sen Gupta, Influence of particle size and shape on their margination and wall-adhesion: implications in drug delivery vehicle design across nano-to-micro scale, Nanoscale, 10 (2018) 15350-15364.
[9] P. Graf, R. Finken, U. Seifert, Adhesion of microcapsules, Langmuir, 22 (2006) 7117-7119.
[10] V. Kudryavtseva, G.B. Sukhorukov, Features of Anisotropic Drug Delivery Systems, Adv Mater, (2023) e2307675.
[11] S. Roh, A.H. Williams, R.S. Bang, S.D. Stoyanov, O.D. Velev, Soft dendritic microparticles with unusual adhesion and structuring properties, Nat Mater, 18 (2019) 1315-1320.
[12] P.T. Spicer, M. Caggioni, J. Lenis-Abril, A.V. Bayles, Non-spherical droplet, Proctor and Gamble, United States, 2013.
[13] X. Lian, S. Liao, W. Han, C. Song, Y. Wang, Stabilizing Liquid in Precise Nonequilibrium Shapes via Fast Interfacial Polymerization, Small, 19 (2023) e2301039.
[14] B.P. Binks, Horozov, T. S., Colloidal Particles at Liquid Interfaces, Cambridge University Press 2006.
[15] B.P. Binks, S.O. Lumsdon, Influence of Particle Wettability on the Type and Stability of Surfactant-Free Emulsions, Langmuir, 16 (2000) 8622-8631.
[16] C. Hao, Z. Xie, T.J. Atherton, P.T. Spicer, Arrested Coalescence of Viscoelastic Droplets: Ellipsoid Shape Effects and Reorientation, Langmuir, 34 (2018) 12379-12386.
[17] A.B. Pawar, M. Caggioni, R. Ergun, R.W. Hartel, P.T. Spicer, Arrested coalescence in Pickering emulsions, Soft Matter, 7 (2011).
[18] C.P. Whitby, E.J. Wanless, Controlling Pickering Emulsion Destabilisation: A Route to Fabricating New Materials by Phase Inversion, Materials (Basel), 9 (2016) 626.
[19] S.A.F. Bon, S.D. Mookhoek, P.J. Colver, H.R. Fischer, S. van der Zwaag, Route to stable non-spherical emulsion droplets, European Polymer Journal, 43 (2007) 4839-4842.
[20] A.B. Subramaniam, M. Abkarian, L. Mahadevan, H.A. Stone, Colloid science: non-spherical bubbles, Nature, 438 (2005) 930.
[21] M. Cui, T. Emrick, T.P. Russell, Stabilizing liquid drops in nonequilibrium shapes by the interfacial jamming of nanoparticles, Science, 342 (2013) 460-463.
[22] J. Forth, X. Liu, J. Hasnain, A. Toor, K. Miszta, S. Shi, P.L. Geissler, T. Emrick, B.A. Helms, T.P. Russell, Reconfigurable Printed Liquids, Adv Mater, 30 (2018) e1707603.
[23] H. Takeoka, H. Hamasaki, Y. Harada, Y. Nakamura, S. Fujii, Synthesis and characterization of polypyrrole-platinum nanocomposite-coated latex particles, Colloid and Polymer Science, 293 (2015) 1483-1493.
[24] M. Hoorfar, W.N. A, Recent progress in axisymmetric drop shape analysis (ADSA), Adv Colloid Interface Sci, 121 (2006) 25-49.

[25] S.M.I. Saad, Z. Policova, A.W. Neumann, Design and accuracy of pendant drop methods for surface tension measurement, Colloids and Surfaces A: Physicochemical and Engineering Aspects, 384 (2011) 442-452.
[26] J.D. Berry, M.J. Neeson, R.R. Dagastine, D.Y. Chan, R.F. Tabor, Measurement of surface and interfacial tension using pendant drop tensiometry, J Colloid Interface Sci, 454 (2015) 226-237.
[27] A.B. Pawar, M. Caggioni, R.W. Hartel, P.T. Spicer, Arrested coalescence of viscoelastic droplets with internal microstructure, Faraday Discuss, 158 (2012) 341-350; discussion 351-370.
[28] B.V. Derjaguin, L. Landau, Theory of the stability of stronglycharged lyophobic sols and of the adhesion of strongly chargedparticles in solution of electrolytes, Acta. Physicochem URSS, 14 (1941) 633.
[29] E.J.W. Verwey, J.T.G. Overbeek, Theory of the Stability ofLyophobic Colloids, The Netherlands, 1948.
[30] F. Ponzio, V. Ball, Polydopamine deposition at fluid interfaces, Polymer International, 65 (2016) 1251-1257.
[31] Y. Liu, K. Ai, L. Lu, Polydopamine and its derivative materials: synthesis and promising applications in energy, environmental, and biomedical fields, Chem Rev, 114 (2014) 5057-5115.
[32] P. Liu, C. Qi, Y. Gao, CTAB-assisted fabrication of well-shaped PDA-based colloidosomes, Colloid and Polymer Science, 297 (2019) 1301-1311.
[33] T.N. Hunter, R.J. Pugh, G.V. Franks, G.J. Jameson, The role of particles in stabilising foams and emulsions, Adv Colloid Interface Sci, 137 (2008) 57-81.
[34] Y. Liu, M. Tourbin, S. Lachaize, P. Guiraud, Silica nanoparticles separation from water: aggregation by cetyltrimethylammonium bromide (CTAB), Chemosphere, 92 (2013) 681-687.
[35] X.-k. Ma, N.-H. Lee, H.-J. Oh, J.-W. Kim, C.-K. Rhee, K.-S. Park, S.-J. Kim, Surface modification and characterization of highly dispersed silica nanoparticles by a cationic surfactant, Colloids and Surfaces A: Physicochemical and Engineering Aspects, 358 (2010) 172-176.
[36] A.J. Kora, R. Manjusha, J. Arunachalam, Superior bactericidal activity of SDS capped silver nanoparticles: Synthesis and characterization, Materials Science and Engineering: C, 29 (2009) 2104-2109.
[37] Y.-C. Lai, C.-S. Lai, J.-T. Tai, T.P. Nguyen, H.-L. Wang, C.-Y. Lin, T.-Y. Tsai, H.-C. Ho, P.-H. Wang, Y.-C. Liao, D.-H. Tsai, Understanding ligand–nanoparticle interactions for silica, ceria, and titania nanopowders, Advanced Powder Technology, 26 (2015) 1676-1686.
[38] S.T. Knox, S. Parkinson, R. Stone, N.J. Warren, Benchtop flow-NMR for rapid online monitoring of RAFT and free radical polymerisation in batch and continuous reactors, Polymer Chemistry, 10 (2019) 4774-4778.
[39] V. Ball, D. Del Frari, V. Toniazzo, D. Ruch, Kinetics of polydopamine film deposition as a function of pH and dopamine concentration: insights in the polydopamine deposition mechanism, J Colloid Interface Sci, 386 (2012) 366-372.
[40] A.T. Tyowua, M. Targema, E.E. Ubuo, Salt-induced edible anisotropic Pickering emulsion droplets, Journal of Dispersion Science and Technology, (2022) 1-12.
[41] J. Gould, G. Garcia-Garcia, B. Wolf, Pickering Particles Prepared from Food Waste, Materials (Basel), 9 (2016).
[42] V.B. Tolstoguzov, A.I. Mzhel'sky, V.Y. Gulov, Deformation of emulsion droplets in flow, Colloid and Polymer Science, 252 (1974) 124-132.
[43] H.J. Karam, J.C. Bellinger, Deformation and Breakup of Liquid Droplets in a Simple Shear Field, Industrial & Engineering Chemistry Fundamentals, 7 (2002) 576-581.
[44] C.P. Whitby, F.E. Fischer, D. Fornasiero, J. Ralston, Shear-induced coalescence of oil-in-water Pickering emulsions, J Colloid Interface Sci, 361 (2011) 170-177.
[45] R. Atkin, V.S. Craig, E.J. Wanless, S. Biggs, Mechanism of cationic surfactant adsorption at the solid-aqueous interface, Adv Colloid Interface Sci, 103 (2003) 219-304.

[46] F. Ponzio, P. Bertani, V. Ball, Role of surfactants in the control of dopamine-eumelanin particle size and in the inhibition of film deposition at solid-liquid interfaces, J Colloid Interface Sci, 431 (2014) 176-179.
[47] A. Cihanoglu, J.D. Schiffman, S. Alsoy Altinkaya, Biofouling-Resistant Ultrafiltration Membranes via Codeposition of Dopamine and Cetyltrimethylammonium Bromide with Retained Size Selectivity and Water Flux, ACS Appl Mater Interfaces, 14 (2022) 38116-38131.
[48] J.K. Ferri, P.A.L. Fernandes, J.T. McRuiz, F. Gambinossi, Elastic nanomembrane metrology at fluid–fluid interfaces using axisymmetric drop shape analysis with anisotropic surface tensions: deviations from Young–Laplace equation, Soft Matter, 8 (2012).
[49] H. Hemmatpour, O. De Luca, D. Crestani, M.C.A. Stuart, A. Lasorsa, P.C.A. van der Wel, K. Loos, T. Giousis, V. Haddadi-Asl, P. Rudolf, New insights in polydopamine formation via surface adsorption, Nat Commun, 14 (2023) 664.
[50] M.J. Qazi, S.J. Schlegel, E.H.G. Backus, M. Bonn, D. Bonn, N. Shahidzadeh, Dynamic Surface Tension of Surfactants in the Presence of High Salt Concentrations, Langmuir, 36 (2020) 7956-7964.
[51] R. Delahaije, L.M.C. Sagis, J. Yang, Impact of Particle Sedimentation in Pendant Drop Tensiometry, Langmuir, 38 (2022) 10183-10191.
[52] F. Chen, Y. Xing, Z. Wang, X. Zheng, J. Zhang, K. Cai, Nanoscale Polydopamine (PDA) Meets pi-pi Interactions: An Interface-Directed Coassembly Approach for Mesoporous Nanoparticles, Langmuir, 32 (2016) 12119-12128.
[53] N. Nishizawa, A. Kawamura, M. Kohri, Y. Nakamura, S. Fujii, Polydopamine Particle as a Particulate Emulsifier, Polymers (Basel), 8 (2016).
[54] E.H. Lucassen-Reynders, A. Cagna, J. Lucassen, Gibbs elasticity, surface dilational modulus and diffusional relaxation in nonionic surfactant monolayers, Colloids and Surfaces A: Physicochemical and Engineering Aspects, 186 (2001) 63-72.
[55] S. Varanasi, L. Henzel, L. Mendoza, R. Prathapan, W. Batchelor, R. Tabor, G. Garnier, Pickering Emulsions Electrostatically Stabilized by Cellulose Nanocrystals, Front Chem, 6 (2018) 409.
[56] J. Krägel, S.R. Derkatch, Interfacial shear rheology, Current Opinion in Colloid & Interface Science, 15 (2010) 246-255.
[57] A.J. Mendoza, E. Guzman, F. Martinez-Pedrero, H. Ritacco, R.G. Rubio, F. Ortega, V.M. Starov, R. Miller, Particle laden fluid interfaces: dynamics and interfacial rheology, Adv Colloid Interface Sci, 206 (2014) 303-319.
[58] K. Yu, H. Zhang, S. Biggs, Z. Xu, O.J. Cayre, D. Harbottle, The rheology of polyvinylpyrrolidone-coated silica nanoparticles positioned at an air-aqueous interface, J Colloid Interface Sci, 527 (2018) 346-355.
[59] G.G. Fuller, J. Vermant, Complex fluid-fluid interfaces: rheology and structure, Annu Rev Chem Biomol Eng, 3 (2012) 519-543.
[60] R. Krishnaswamy, S. Majumdar, R. Ganapathy, V.V. Agarwal, A.K. Sood, C.N. Rao, Interfacial rheology of an ultrathin nanocrystalline film formed at the liquid/liquid interface, Langmuir, 23 (2007) 3084-3087.
[61] C. DeArmitt, S.P. Armes, Colloidal dispersions of surfactant-stabilized polypyrrole particles, Langmuir, 9 (2002) 652-654.
[62] J. Hazarika, A. Kumar, Controllable synthesis and characterization of polypyrrole nanoparticles in sodium dodecylsulphate (SDS) micellar solutions, Synthetic Metals, 175 (2013) 155-162.
[63] S. Fujii, S. Matsuzawa, Y. Nakamura, A. Ohtaka, T. Teratani, K. Akamatsu, T. Tsuruoka, H. Nawafune, Synthesis and characterization of polypyrrole-palladium nanocomposite-coated latex particles and their use as a catalyst for Suzuki coupling reaction in aqueous media, Langmuir, 26 (2010) 6230-6239.
[64] M. Šišáková, Y. Asaumi, M. Uda, M. Seike, K. Oyama, S. Higashimoto, T. Hirai, Y. Nakamura, S. Fujii, Dodecyl sulfate-doped polypyrrole derivative grains as a light-responsive liquid marble stabilizer, Polymer Journal, 52 (2020) 589-599.

[65] S. Xing, G. Zhao, Morphology, structure, and conductivity of polypyrrole prepared in the presence of mixed surfactants in aqueous solutions, Journal of Applied Polymer Science, 104 (2007) 1987-1996.
[66] S. Horiuchi, Y. Nakao, Platinum colloid catalyzed etchingless gold electroless plating with strong adhesion to polymers, Surface and Coatings Technology, 204 (2010) 3811-3817.
[67] J. Hitchcock, A.L. White, N. Hondow, T.A. Hughes, H. Dupont, S. Biggs, O.J. Cayre, Metal-shell nanocapsules for the delivery of cancer drugs, J Colloid Interface Sci, 567 (2020) 171-180.